THE JOURNAL OF PHYSICAL CHEMISTRY B
A JOURNAL OF THE AMERICAN CHEMICAL SOCIETY

pubs.acs.org/JPCB

Article

DFT-Based Calculation of Molecular Hyperpolarizability and SFG Intensity of Symmetric and Asymmetric Stretch Modes of Alkyl Groups

Juseok Choi, Albert L. Kwansa, Yaroslava G. Yingling, and Seong H. Kim*

Cite This: J. Phys. Chem. B 2023, 127, 8456–8467

Read Online

ACCESS | Metrics & More | Article Recommendations | Supporting Information

ABSTRACT: Vibrational sum frequency generation (SFG) spectroscopy has been extensively used for obtaining structural information of molecular functional groups at two-dimensional (2D) interfaces buried in the gas or liquid medium. Although the SFG experiment can be done elegantly, interpreting the measured intensity in terms of molecular orientation with respect to the lab coordinate is quite complicated. One of the main reasons is the difficulty of determining the hyperpolarizability tensors of even simple molecules that govern their SFG responses. The single-bond polarizability derivative model has been proposed to estimate the relative magnitude of SFG-active hyperpolarizability by assuming that the perturbation associated to each vibration is negligible. In this study, density functional theory was used to calculate the polarizability and dipole derivative tensors of the CH_3 stretch mode of CH_3I, CH_3CH_2I, CH_3OH, and CH_3CH_2OH. Then, the hyperpolarizability tensors of symmetric and asymmetric vibration modes were calculated considering the Boltzmann distribution of representative conformers, which allowed us to theoretically calculate their SFG intensities at all polarization combinations as a function of the tilt angle of the CH_3 group with respect to the surface normal direction. Then, the ratios of the calculated SFG intensities for the CH_3 symmetric and asymmetric stretch peaks used in experimental studies for the CH_3 tilt angle determination were compared. This comparison clearly showed that the effect of vibrational coupling among neighboring functional groups is significant and cannot be assumed to be negligible. This study presents new parameters that can be used in determining the average tilt angle of the CH_3 group at the 2D interface with SFG measurements as well as limitations of the method.

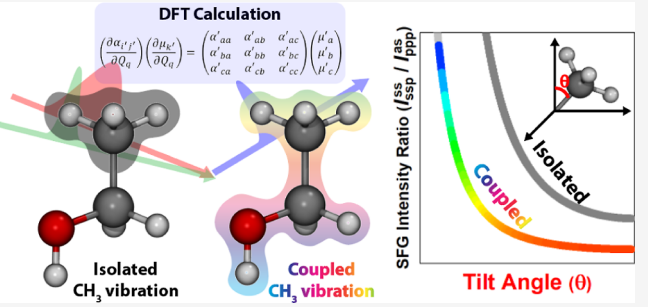

INTRODUCTION

Sum frequency generation (SFG) vibrational spectroscopy has been instrumental in elucidating structural orders of molecular functional groups at two-dimensional (2D) interfaces such as solid/gas, solid/liquid, liquid/gas, and liquid/liquid phase boundaries,[1−4] which enabled fundamental studies of chemical reactions and physical interactions occurring at heterogeneous catalyst surfaces, thin films, biological membranes, emulsion processes, and so on.[5−8] This is because the SFG process requires noncentrosymmetry,[2,4] and the interface of two bulk phases naturally produces the noncentrosymmetric condition along the direction normal to the phase boundary. SFG spectroscopy is also a powerful analytical tool to unveil three-dimensional (3D) structural orders of various crystalline biopolymers, such as collagen, cellulose, chitin, amylose, and so forth, interspersed in amorphous matrices,[9−12] if the crystal structure is noncentrosymmetric. In all these studies, the structural order information is obtained or deduced by comparing experimentally measured SFG intensities with either the data from a model system with a well-controlled geometry or the theoretical calculation results.[5,13−16]

The SFG intensity of a specific vibrational mode can be calculated for a given molecular orientation with respect to the lab coordinate using its molecular hyperpolarizability tensor, $\beta_{i',j',k'}$ where i', j', and k' are the molecular coordinates (see the Methods section for details).[17,18] Thus, if the relative magnitudes of $\beta_{i',j',k'}$ tensor elements are known, it is possible to determine the molecular orientation from SFG measurements.[17,18] In SFG studies of organic molecules at optically flat 2D interfaces with the C_∞ symmetry (i.e., isotropic within the 2D plane), the vibrational modes of alkyl groups in the 2800−3000 cm^{-1} region have been extensively used to determine the tilt angle (θ) of interfacial molecules with respect to the surface normal direction.[13,19] If the modes detected in this spectral

Received: June 9, 2023
Revised: August 2, 2023
Published: September 25, 2023

https://doi.org/10.1021/acs.jpcb.3c03910
J. Phys. Chem. B 2023, 127, 8456−8467

region are assumed to be the stretch modes of CH_2 and CH_3 groups that are not coupled with vibrations of other groups in the molecule, then the relative magnitudes of SFG-active $\beta_{i',j',k'}$ elements (often called hyperpolarizability ratio, R) could be estimated using the single-bond polarizability derivative (SBPD) ratio (r) and the bond angle (τ) of the local molecular symmetry (i.e., C_{2v} for CH_2 or C_{3v} for CH_3).[17,20] This is called the SBPD model. Under the same assumption, the r value can be estimated from the experimentally measured Raman depolarization ratio (ρ) and τ.[17,21−24]

The SBPD model was established by Hirose et al. who assumed that the perturbation of the CH_2 and CH_3 vibrational modes from the local molecular symmetry is rather insignificant.[20,21] Within this assumption, the CH_2 and CH_3 vibrational modes should meet the symmetry rules of the C_{2v} and C_{3v} point groups, respectively.[25,26] This assumption was necessary in their seminal work in the early 1990s due to the difficulty of estimating all components of Raman tensors from the limited experimental data.[21] Recently, it was shown experimentally that, for the CH_3 symmetric stretch mode, the r value varies depending on the neighboring group to which the CH_3 group is attached.[27] This is due to the coupling of vibrational modes with neighboring groups as well as the Fermi resonance with overtones of their bending modes.[28−30] Such couplings make it difficult (if not impossible) to predict the magnitudes of SFG-active elements in the hyperpolarizability $\beta_{i',j',k'}$ tensor from the SBPD model.

In this study, we have used density functional theory (DFT) calculations to predict the polarizability and dipole derivative tensors, $\frac{\partial \alpha_{i'j'}}{\partial Q_q}$ and $\frac{\partial \mu_{k'}}{\partial Q_q}$, respectively, of the alkyl stretch modes of CH_3I, CH_3CH_2I, CH_3OH, and CH_3CH_2OH, which were then used to calculate the full $\beta_{i',j',k'}$ tensors of each vibrational mode and then the polarization and tilt angle dependencies of the SFG intensity of the normal modes involving the stretch vibrations of the CH_3 group. CH_3I was chosen since it meets the perfect C_{3v} symmetry. Among various halides, iodide was chosen because its atomic mass is ∼10 times larger than that of carbon, thus making the vibrational coupling smaller. In CH_3CH_2I, the CH_3 and CH_2 vibrations are coupled, so the C_{3v} symmetry assumption is no longer valid to describe the normal modes involving symmetric and asymmetric CH_3 stretches. In CH_3OH, the asymmetric stretch of CH_3 is affected by the dipole of OH. In CH_3CH_2OH, the stretch modes of the CH_3, CH_2, and OH groups are all coupled. Due to computational complexity and limitations,[31,32] vibrational relaxation dynamics and Fermi resonance were not considered in the current study. Although this may affect the accuracy of the DFT-calculated $\beta_{i',j',k'}$ tensors, this study can still show how the polarization and tilt angle dependence of the SFG signal will vary due to vibrational coupling among neighboring groups. This work focuses on the CH_3 and CH_3CH_2 groups at the 2D interface with the C_∞ symmetry only; nonetheless, the same principle and approach can be employed to analyze the orientational distribution of more complicated molecules in both 2D and 3D systems using computational approaches.[18,33−35]

METHODS

The SFG signal intensity (I_{SFG}) is proportional to the square of the effective second-order nonlinear susceptibility ($\chi^{(2)}_{eff}$) and the intensities of two input beams, one of which is the frequency up-conversion beam (I_{VIS}) and the other is the mid-IR beam (I_{IR}) resonating with a specific vibrational absorption band[18]

$$I_{SFG} \propto |\chi^{(2)}_{eff}|^2 I_{VIS} I_{IR} \tag{1}$$

Here, the $\chi^{(2)}_{eff}$ term includes the Fresnel coefficient factors (C_{Fres}) and the electric field vector projections ($\hat{e}_{proj}$) of three polarized beams (SFG, VIS, and IR) and the second-order susceptibility of the SFG-active vibrational mode ($\chi^{(2)}_{ijk}$) (their equations used here are described in ref 18)

$$\chi^{(2)}_{eff} = \sum_{i,j,k=X,Y,Z} C_{Fres}\hat{e}_{proj}\chi^{(2)}_{ijk} \tag{2}$$

$\chi^{(2)}_{ijk}$ is the third-rank tensor, which can be related to the molecular hyperpolarizability tensor ($\beta_{i',j',k'}$) through[18]

$$\chi^{(2)}_{ijk} \propto N \sum_{i',j',k'=a,b,c} \frac{\langle R_{ii'}R_{jj'}R_{kk'}\beta_{i',j',k'}\rangle}{\omega_{IR} - \omega_q + i\Gamma_q} \tag{3}$$

where N is the number density of the SFG-active modes, $R_{ii'}R_{jj'}R_{kk'}$ is the product of Euler matrices transforming the i', j', k' molecular coordinate (a, b, c) to the i, j, k lab coordinate (X, Y, Z), ω_{IR} is the wavenumber of the IR beam, and ω_q and Γ_q are the resonant wavenumber and damping factor of the qth normal mode. Here, the Euler matrix term is expressed with the polar coordinate angles (θ, ϕ, ψ) describing the relative orientation of the principal axes of (a, b, c) with respect to those of (X, Y, Z), where θ, ϕ, and ψ are called tilt, azimuth, and twist angles, respectively.[17] In eq 3, $\beta_{i',j',k'}$ is proportional to the product of the polarizability $\left(\frac{\partial \alpha_{i'j'}}{\partial Q_q}\right)$ and dipole $\left(\frac{\partial \mu_{k'}}{\partial Q_q}\right)$ derivatives along the normal mode coordinate (Q_q), which can be expressed in the following matrix form[35,36]

$$\left(\frac{\partial \alpha_{i'j'}}{\partial Q_q}\right) = \begin{pmatrix} \alpha'_{aa} & \alpha'_{ab} & \alpha'_{ac} \\ \alpha'_{ba} & \alpha'_{bb} & \alpha'_{bc} \\ \alpha'_{ca} & \alpha'_{cb} & \alpha'_{cc} \end{pmatrix} \text{ and } \left(\frac{\partial \mu_{k'}}{\partial Q_q}\right) = \begin{pmatrix} \mu'_a \\ \mu'_b \\ \mu'_c \end{pmatrix} \tag{4}$$

If the functional group of interest is CH_3, the c axis of the molecular coordinate is set to the three-fold rotational axis of the C_{3v} symmetry group, and a and b are two principal axes orthogonal to the c axis. Then, the $\beta_{i',j',k'}$ tensor has the following format

$$\beta_{i',j',k'} = \begin{pmatrix} \begin{pmatrix} \beta_{aaa} \\ \beta_{aab} \\ \beta_{aac} \end{pmatrix} & \begin{pmatrix} \beta_{aba} \\ \beta_{abb} \\ \beta_{abc} \end{pmatrix} & \begin{pmatrix} \beta_{aca} \\ \beta_{acb} \\ \beta_{acc} \end{pmatrix} \\ \begin{pmatrix} \beta_{baa} \\ \beta_{bab} \\ \beta_{bac} \end{pmatrix} & \begin{pmatrix} \beta_{bba} \\ \beta_{bbb} \\ \beta_{bbc} \end{pmatrix} & \begin{pmatrix} \beta_{bca} \\ \beta_{bcb} \\ \beta_{bcc} \end{pmatrix} \\ \begin{pmatrix} \beta_{caa} \\ \beta_{cab} \\ \beta_{cac} \end{pmatrix} & \begin{pmatrix} \beta_{cba} \\ \beta_{cbb} \\ \beta_{cbc} \end{pmatrix} & \begin{pmatrix} \beta_{cca} \\ \beta_{ccb} \\ \beta_{ccc} \end{pmatrix} \end{pmatrix} = \begin{pmatrix} \begin{pmatrix} \alpha'_{aa}\mu'_a \\ \alpha'_{aa}\mu'_b \\ \alpha'_{aa}\mu'_c \end{pmatrix} & \begin{pmatrix} \alpha'_{ab}\mu'_a \\ \alpha'_{ab}\mu'_b \\ \alpha'_{ab}\mu'_c \end{pmatrix} & \begin{pmatrix} \alpha'_{ac}\mu'_a \\ \alpha'_{ac}\mu'_b \\ \alpha'_{ac}\mu'_c \end{pmatrix} \\ \begin{pmatrix} \alpha'_{ba}\mu'_a \\ \alpha'_{ba}\mu'_b \\ \alpha'_{ba}\mu'_c \end{pmatrix} & \begin{pmatrix} \alpha'_{bb}\mu'_a \\ \alpha'_{bb}\mu'_b \\ \alpha'_{bb}\mu'_c \end{pmatrix} & \begin{pmatrix} \alpha'_{bc}\mu'_a \\ \alpha'_{bc}\mu'_b \\ \alpha'_{bc}\mu'_c \end{pmatrix} \\ \begin{pmatrix} \alpha'_{ca}\mu'_a \\ \alpha'_{ca}\mu'_b \\ \alpha'_{ca}\mu'_c \end{pmatrix} & \begin{pmatrix} \alpha'_{cb}\mu'_a \\ \alpha'_{cb}\mu'_b \\ \alpha'_{cb}\mu'_c \end{pmatrix} & \begin{pmatrix} \alpha'_{cc}\mu'_a \\ \alpha'_{cc}\mu'_b \\ \alpha'_{cc}\mu'_c \end{pmatrix} \end{pmatrix} \tag{5}$$

https://doi.org/10.1021/acs.jpcb.3c03910
J. Phys. Chem. B 2023, 127, 8456−8467

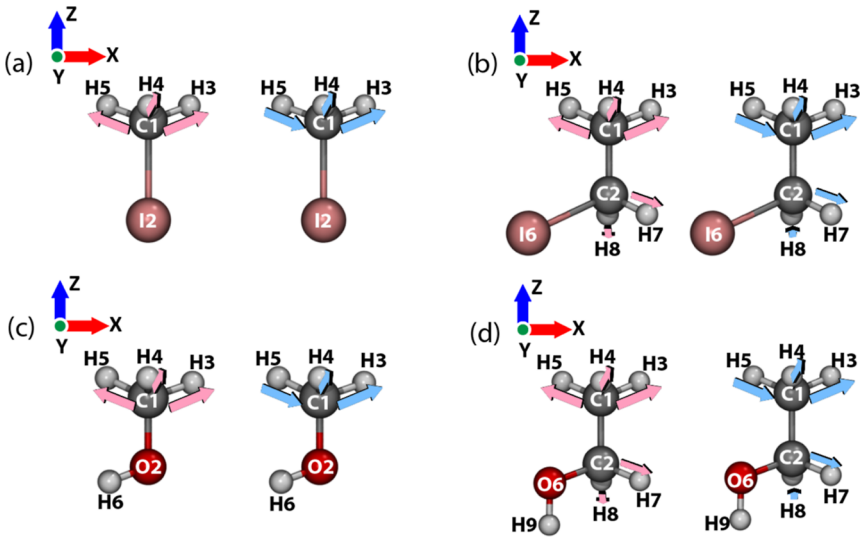

Figure 1. Schematic illustration of vibrational modes of (a) methyl iodide, (b) ethyl iodide, (c) methanol, and (d) ethanol calculated with *Gaussian 16*. Only the modes with the largest contributions from symmetric and asymmetric CH_3 stretching of each molecule are shown graphically with displacement vectors. Movies of all normal modes involving alkyl group stretching are shown in the Movies 1, 2, 3, and 4 of the Supporting Information.

The $\left(\frac{\partial \alpha_{i'j'}}{\partial Q_q}\right)$ and $\left(\frac{\partial \mu_{k'}}{\partial Q_q}\right)$ tensors can be obtained from DFT calculations. We have used the Gaussian 16 software[37] to calculate the normal modes and the associated tensors for each mode for CH_3I, CH_3CH_2I, CH_3OH, and CH_3CH_2OH. For carbon, hydrogen, and oxygen atoms, the Becke, three-parameter, Lee−Yang−Parr (B3LYP) hybrid DFT functional, and Pople's 6-311++G(d,p) basis set were used for the main DFT calculations.[37−39] This basis set includes 6 core basis functions ("6"), triple-split-valence basis functions ("311"), polarization functions for both heavy and light atoms ("d,p"), and diffuse functions for heavy and light atoms ("++"). Using CH_3OH and CH_3CH_2OH, an assessment of convergence criteria (default, "Tight", or "VeryTight") was conducted with B3LYP/6-311++G(d,p), and an assessment of basis set size was conducted with the "Tight" convergence criteria (see Figure S1 in the Supporting Information). For iodine, the B3LYP functional and the Los Alamos effective core potential (ECP) for core with double-zeta for valence (LanL2DZ) basis set were used.[40] The Stuttgart/Dresden ECP for core with double-zeta for valence SDD basis set was also tested using CH_3I and CH_3CH_2I (Figure S2).[41] The Gaussian 16 convergence criteria include maximum force, root-mean-square (rms) force, maximum displacement, and rms displacement; the "Tight" criteria are 30 times stricter compared to the default criteria, and the "VeryTight" criteria are up to 300 times stricter compared to the default criteria.

The following four-stage DFT workflow was used: (1) a geometry optimization with no constraints on atom positions, (2) a two-step molecular alignment along the *Z*-axis using C1−C2 for CH_3CH_2OH and CH_3CH_2I, C1−O for CH_3OH, and C1−I for CH_3I followed by C1−H4 aligned with the *YZ* plane (see Figure 1), (3) a geometry optimization with generalized internal coordinates (GICs) (e.g., freezing the *X* and *Y* coordinates of C1 and C2 and the X coordinate of H4), and (4) a frequency calculation with no constraints on atom positions. The default integration grid size ("UltraFine") and the "Tight" optimization convergence criteria were used while calculating the Hessian matrix analytically for both geometry optimization stages ("Opt = (CalcAll, Tight)"). For each molecule, the order of vibrational peak positions was checked to be consistent with experimental data or previously published DFT results (Table S1 in the Supporting Information).[18] For each of the eclipsed conformers of CH_3OH, an additional GIC was added for the H−C−O−H dihedral angle (setting to ~0°) during stages 1 and 3 to prevent relaxing to the more stable staggered conformation. For the dipole derivative calculation, two displacements were applied from the geometry-optimized position along each Cartesian direction with a default step size of 0.001 Å. For the polarizability derivative calculation, an electric field was applied with a default step size of 0.001 au along each Cartesian direction.[42]

A series of method development DFT calculations was initially conducted that led to the final set of conditions (e.g., "Tight" convergence criteria, GICs, chosen basis sets, and analytic Hessian calculation for the optimization stages) and the workflow (four stages) employed for the main set of DFT calculations. These conditions and workflow allowed for a complete convergence at all DFT stages with no imaginary frequencies for all systems except for the three eclipsed CH_3OH conformers (one imaginary frequency each, which was expected due to the additional dihedral GIC needed to maintain each eclipsed conformation).

Vibrational energies in the wavenumber (cm^{-1}) unit, dipole derivatives in the $\sqrt{km/mol}$ unit, and polarizability derivatives in the $\sqrt{Å^4/amu}$ unit were obtained from the Gaussian 16 frequency calculation output. Normal mode visualizations were generated with GaussView 6.[43] IR and Raman spectra (with the intensity unit of km/mol and $Å^4$/amu, respectively) were generated with GaussSum 3.0 using a vibrational energy range of 0−4000 cm^{-1}, 500 data points, a full width at half-maximum (fwhm) of 10 cm^{-1}, and a vibrational energy scaling factor of 1.0 (all default values for GaussSum).[44] The vibrational energies were calculated from the Hessian matrix. The IR intensity was calculated as the sum of squares of the three dipole derivatives, while the Raman activity was calculated from the mean of the diagonal polarizability derivatives (α'_p) and the anisotropy of the polarizability derivatives (γ'_p) as $45 \times \alpha'^2_p + 7 \times \gamma'^2_p$.[45] The IR and Raman spectra were calculated based on a convolution using

https://doi.org/10.1021/acs.jpcb.3c03910
J. Phys. Chem. B 2023, 127, 8456−8467

Table 1. Polarizability and Dipole Derivative Tensors of CH_3I and CH_3CH_2I[a]

	CH_3^s	CH_3^{as}
CH_3I	$\begin{pmatrix}-1.68 & 0.00 & 0.00\\ 0.00 & -1.68 & 0.00\\ 0.00 & 0.00 & -1.75\end{pmatrix}\begin{pmatrix}0.00\\ 0.00\\ 3.71\end{pmatrix}$	$\begin{pmatrix}0.46 & 0.87 & 1.18\\ 0.87 & -0.47 & 0.63\\ 1.18 & 0.63 & 0.00\end{pmatrix}\begin{pmatrix}-1.14\\ -0.61\\ 0.00\end{pmatrix}$
	CH_3^s coupled with CH_2	CH_3^{as} coupled with CH_2
CH_3CH_2I ($\delta = 60°$)	$\begin{pmatrix}2.58 & 0.74 & 1.29\\ 0.74 & 1.67 & 0.72\\ 1.29 & 0.72 & 2.17\end{pmatrix}\begin{pmatrix}-2.55\\ -1.43\\ -3.73\end{pmatrix}$	$\begin{pmatrix}0.90 & -0.55 & -0.74\\ -0.55 & -0.90 & 1.31\\ -0.74 & 1.31 & 0.00\end{pmatrix}\begin{pmatrix}1.60\\ -2.84\\ -0.01\end{pmatrix}$

[a]The three-fold rotation axis of the CH_3 group is aligned with the (vertical) Z-axis of the lab coordinate and the C1−H4 atoms are in the YZ plane. In the case of CH_3CH_2I, the H4−C1−C2−I6 dihedral angle (δ) is 60°. The (3 × 3) matrix is $\left(\frac{\partial \alpha_{i'j'}}{\partial Q_q}\right)$, and the (3 × 1) matrix is $\left(\frac{\partial \mu_{k'}}{\partial Q_q}\right)$.

the Lorentzian function as follows: $y(x) = \sum_{i=1}^{N} \frac{(\text{height}_i \cdot a)}{(\text{position}_i - x)^2 + a}$, where a = fwhm^2/4, i = normal mode number, and N = total number of normal modes.[46] The single-molecule IR and Raman spectra of each case are shown in Figure S3 in the Supporting Information.

In addition, we have calculated and compared the polarizability tensors with both static and time-dependent (TD) DFT methods. The Raman spectra calculated with static-DFT and those with TD-DFT at 300−1000 nm excitations (every 100 nm) are shown in Figure S4 in the Supporting Information. Obviously, there were some differences in relative intensities among the calculation results, but the differences were negligible. This was because the frequency up-conversion beam (I_{VIS}) was not resonating with electronic excitation to the antibonding orbital of the molecules studied here.[47] Thus, the use of TD-DFT would not affect the SFG intensity calculation; for simplicity, we employed the static-DFT results in this study.

For the molecular conformation in DFT calculations, we considered the most stable conformer and the next stable conformer whose energy was within ∼5 kJ/mol from the lowest energy conformation. Based on the Boltzmann distribution, the population of the conformer with ∼5 kJ/mol higher energy will be only ∼10% of the lowest energy conformer at room temperature. In the case of methanol, both staggered and eclipsed conformations for the C−H and O−H groups were considered ($\Delta E \approx 4.4$ kJ/mol; see Figure S5). In the case of ethanol, the eclipsed conformers were ignored, and the staggered conformers with the OH group in the trans and gauche with respect to the CH_3 group were considered ($\Delta E \approx 0.3$ kJ/mol).[48] In the case of ethyl iodide, only the staggered conformer was considered for simplicity.[49]

After getting $\left(\frac{\partial \alpha_{i'j'}}{\partial Q_q}\right)$ and $\left(\frac{\partial \mu_{k'}}{\partial Q_q}\right)$ of each conformer, the full set of $\beta_{i',j',k'}$ was calculated using eq 5. Then, the statistically weighted average was calculated with the consideration of the Boltzmann distribution of various conformers as well as all possible dihedral angles within the molecular coordinate. For conformers with a different dihedral angle (δ) with respect to the C1−H4 atoms in the YZ plane, the $\beta_{i',j',k'}$ tensors could be calculated by the Euler transformation from the $\left(\frac{\partial \alpha_{i'j'}}{\partial Q_q}\right)$ and $\left(\frac{\partial \mu_{k'}}{\partial Q_q}\right)$ tensors generated from the original DFT calculation. An example of calculating the derivative tensors of two rotational conformers of methanol with dihedral angles of 180 and 300° from the tensors of the conformer with the 60° dihedral angle while keeping the C1−H4 atoms in the YZ plane is shown in Figure S6 in the Supporting Information.

Once the full set of $\beta_{i',j',k'}$ is properly averaged, then $\chi^{(2)}_{ijk}$ can be calculated for any given tilt angle (θ) of the CH_3 group with respect to the lab coordinate using eq 3. Reflecting the C_∞ symmetry of the 2D interface, the random distributions of twisting (ψ) and azimuth (ϕ) angles of molecules with respect to the lab coordinate were imposed by integrating over all possible ψ and ϕ angles (0 to 2π). For simplicity, we first discuss the results from calculations done without considering the tilt angle distribution (i.e., assuming the delta function). Then, the effect of the Gaussian distribution of the molecular tilt angle is shown at the end.[4,19]

Finally, the $\chi^{(2)}_{eff}$ terms for any given polarization combinations were calculated with eq 2 at given incidence angles of I_{VIS} and I_{IR}. The refractive index values were taken from ref 17. The polarization is represented by a combination of three characters (p or s with respect to the laser incidence plane) in the order of SFG signal, up-conversion beam, and mid-IR beam from left to right. For example, the ssp polarization means the SFG signal is detected in the s-polarization when the input visible and IR polarizations are s and p, respectively. The numerical calculations were done with Mathematica. Since Mathematica can handle all 27 $\beta_{i',j',k'}$ elements, it was not necessary to select specific terms based on the C_∞ symmetry of the 2D interface; the symmetry-forbidden terms were naturally cancelled out. The full Mathematica program is given in the Supporting Information, which calculates the I_{SFG} through eqs 1−5 as a function of the CH_3 tilt angle (θ) for all polarization combinations and given incidence angles of I_{VIS} and I_{IR} using the $\left(\frac{\partial \alpha_{i'j'}}{\partial Q_q}\right)$ and $\left(\frac{\partial \mu_{k'}}{\partial Q_q}\right)$ tensors obtained from DFT calculations.

RESULTS AND DISCUSSION

Normal Vibrational Modes from DFT. Figure 1 illustrates the vibrational modes involving symmetric and asymmetric stretches of the CH_3 group of each molecule (Movies 1, 2, 3, and 4 are shown in the Supporting Information). Only two major modes with high intensities in the SFG calculation are shown here. These are most relevant to the experimental work, which corresponds to the symmetric stretch peak at 2860−2880 cm^{-1} observed in the ssp polarization and the asymmetric stretch peak at 2960−2980 cm^{-1} in the ppp and sps polarizations.[50] The CH_3 stretch modes of methyl iodide (Figure 1a) perfectly fit to the C_{3v} point group.[25] In contrast, the CH_3 stretch modes of ethyl iodide are coupled with the CH_2 stretch modes (Figure 1b). That is because they are covalently connected, and their masses

https://doi.org/10.1021/acs.jpcb.3c03910
J. Phys. Chem. B 2023, 127, 8456−8467

are quite close to each other. In the case of methanol, the CH_3 stretch modes are coupled with a slight movement of the OH group (Figure 1c). With respect to the center of mass of the molecule, the C1−O2 bond length slightly changes in response to the symmetric CH_3 stretch. The asymmetric CH_3 stretch is coupled with the C1−O2 tilt or O2−H6 stretch depending on the phase between the asymmetric stretch dipole and the C1−O2−H6 plane. In the case of ethyl alcohol, the CH_3 stretch modes are coupled with the CH_2 stretch modes, which are coupled with the OH modes as well (Figure 1d).

In the following sections, the two iodide cases will be discussed first to show how the CH_3 and CH_2 coupling affects the polarization and tilt angle dependence of the SFG signal. Then, the two alcohol cases will be discussed to see further impacts due to the involvement of OH groups. Finally, the tilt angle dependence of the theoretically calculated SFG signals will be compared with the experimental data, and suggestions for analysis of other alkyl groups in hydrocarbon or polymer surfaces will be made.

SFG Calculations for Methyl Iodide and Ethyl Iodide.

Table 1 shows the $\left(\frac{\partial \alpha_{i'j'}}{\partial Q_q}\right)$ and $\left(\frac{\partial \mu_{k'}}{\partial Q_q}\right)$ tensors in a matrix form. In the C_{3v} point group, the A_1 mode (which is the symmetric stretch) has two Raman-active components perpendicular ($a^2 + b^2$) and parallel (c^2) to the molecular axis and one IR-active component along the molecular axis (c).[26] Consistently, for the symmetric stretch mode of CH_3I, the polarizability and dipole derivative tensors have non-zero values only in $\alpha'_{aa} = \alpha'_{bb} \neq \alpha'_{cc}$ and μ'_c, respectively. The asymmetric stretch of CH_3I is the E mode in the C_{3v} point group, in which the ab, bc, ac, and $a^2 - b^2$ components are Raman-active, and the a and b components are IR-active.[26] Thus, its polarizability and dipole derivatives have non-zero values in all terms, except α'_{cc} and μ'_c. In Table 1, only one of the energetically degenerate E modes of CH_3I is shown ($|\mu'_a| > |\mu'_b|$); the other one is orthogonal to this one and its dipole derivative has $|\mu'_a| < |\mu'_b|$.

For ethyl iodide, the distribution of non-zero values in the polarizability and dipole derivative tensors of the two normal modes with dominant contributions from the symmetric and asymmetric stretches of the terminal CH_3 group is quite different from those of methyl iodide. In the symmetric mode of ethyl iodide, all terms in the polarizability and dipole tensors have non-zero values. This is because the coupling with the symmetric CH_2 stretch breaks the three-fold rotational symmetry of the symmetric stretch of CH_3. Similarly, the asymmetric mode of ethyl iodide has a non-zero μ'_c term, although it is small. All these differences are due to the vibrational coupling of the CH_3 and CH_2 groups.

Table 2 lists the relative magnitudes of all terms in the molecular hyperpolarizability $\beta_{i',j',k'}$ tensor calculated from the polarizability $\left(\frac{\partial \alpha_{i'j'}}{\partial Q_q}\right)$ and dipole $\left(\frac{\partial \mu_{k'}}{\partial Q_q}\right)$ derivatives using eq 5 with consideration of different conformers with energetically stable dihedral angles in the molecular coordinate. In the case of CH_3I, which has the perfect C_{3v} symmetry, only $\beta_{aac} = \beta_{bbc}$ and β_{ccc} have non-zero values in the symmetric stretch, as discussed in the SBPD model.[17] In the asymmetric mode, the non-zero elements are $\beta_{aca} = \beta_{bcb} = \beta_{caa} = \beta_{cbb}$ (=0.27) and $\beta_{aab} = \beta_{aba} = \beta_{baa} = -\beta_{bbb}$ (=0.20, which is equivalent to $\beta_{aaa} = -\beta_{aab} = -\beta_{bba} = -\beta_{bab}$ with switching of the a and b directionality), as expected from the C_{3v} symmetry.[17] This is due to the cancellation of two orthogonal asymmetric modes that are energetically degenerate (see Movies 1, 2, 3, and 4 in the Supporting Information).

Table 2. Hyperpolarizability $\beta_{i',j',k'}$ Tensors of CH_3I and CH_3CH_2I[a]

	CH_3^s			CH_3^{as}		
CH_3I	$\begin{pmatrix}0.00\\0.00\\\mathbf{0.96}\end{pmatrix}$	$\begin{pmatrix}0.00\\0.00\\0.00\end{pmatrix}$	$\begin{pmatrix}0.00\\0.00\\0.00\end{pmatrix}$	$\begin{pmatrix}0.00\\\mathbf{0.20}\\0.00\end{pmatrix}$	$\begin{pmatrix}\mathbf{0.20}\\0.00\\0.00\end{pmatrix}$	$\begin{pmatrix}\mathbf{0.27}\\0.00\\0.00\end{pmatrix}$
	$\begin{pmatrix}0.00\\0.00\\0.00\end{pmatrix}$	$\begin{pmatrix}0.00\\0.00\\\mathbf{0.96}\end{pmatrix}$	$\begin{pmatrix}0.00\\0.00\\0.00\end{pmatrix}$	$\begin{pmatrix}\mathbf{0.20}\\0.00\\0.00\end{pmatrix}$	$\begin{pmatrix}0.00\\\mathbf{-0.20}\\0.00\end{pmatrix}$	$\begin{pmatrix}0.00\\\mathbf{0.27}\\0.00\end{pmatrix}$
	$\begin{pmatrix}0.00\\0.00\\0.00\end{pmatrix}$	$\begin{pmatrix}0.00\\0.00\\0.00\end{pmatrix}$	$\begin{pmatrix}0.00\\0.00\\\mathbf{1.00}\end{pmatrix}$	$\begin{pmatrix}\mathbf{0.27}\\0.00\\0.00\end{pmatrix}$	$\begin{pmatrix}0.00\\\mathbf{0.27}\\0.00\end{pmatrix}$	$\begin{pmatrix}0.00\\0.00\\0.00\end{pmatrix}$
	CH_3^s coupled with CH_2			CH_3^{as} coupled with CH_2		
CH_3CH_2I	$\begin{pmatrix}0.01\\0.16\\\mathbf{0.98}\end{pmatrix}$	$\begin{pmatrix}0.16\\-0.01\\0.00\end{pmatrix}$	$\begin{pmatrix}0.27\\0.00\\0.00\end{pmatrix}$	$\begin{pmatrix}0.01\\\mathbf{0.21}\\0.00\end{pmatrix}$	$\begin{pmatrix}\mathbf{0.21}\\-0.01\\0.00\end{pmatrix}$	$\begin{pmatrix}\mathbf{0.30}\\0.00\\0.00\end{pmatrix}$
	$\begin{pmatrix}0.16\\-0.01\\0.00\end{pmatrix}$	$\begin{pmatrix}-0.01\\-0.16\\\mathbf{0.98}\end{pmatrix}$	$\begin{pmatrix}0.00\\0.27\\0.00\end{pmatrix}$	$\begin{pmatrix}\mathbf{0.21}\\-0.01\\0.00\end{pmatrix}$	$\begin{pmatrix}-0.01\\\mathbf{-0.21}\\0.00\end{pmatrix}$	$\begin{pmatrix}0.00\\\mathbf{0.30}\\0.00\end{pmatrix}$
	$\begin{pmatrix}0.27\\0.00\\0.00\end{pmatrix}$	$\begin{pmatrix}0.00\\0.27\\0.00\end{pmatrix}$	$\begin{pmatrix}0.00\\0.00\\\mathbf{1.00}\end{pmatrix}$	$\begin{pmatrix}\mathbf{0.30}\\0.00\\0.00\end{pmatrix}$	$\begin{pmatrix}0.00\\\mathbf{0.30}\\0.00\end{pmatrix}$	$\begin{pmatrix}0.00\\0.00\\0.00\end{pmatrix}$

[a]The three-fold rotation axis of the methyl group is aligned with the (vertical) Z-axis of the lab coordinate. The tensor elements of the asymmetric CH_3I stretch are the sum of two energetically degenerate modes whose dipole derivatives are orthogonal (a and b). The tensor elements of CH_3CH_2I are the average of three staggered conformers (δ = 60, 180, 300°). The bold numbers are the elements expected to be large based on the perfect C_{3v} symmetry. All values are normalized with the β_{ccc} component of the CH_3 symmetric stretch mode. The tensor elements of individual conformers are shown in Table S2 in the Supporting Information to show how different contributions cancel out.

In the case of CH_3CH_2I, one can see non-zero values in the hyperpolarizability elements that are expected to be zero if the vibrational mode adheres strictly to the C_{3v} point group. The deviation from the ideal C_{3v} case is larger for the symmetric mode than the asymmetric mode. Again, this is due to the coupling between CH_3 and CH_2 groups.

Once all 27 molecular hyperpolarizability terms ($\beta_{i',j',k'}$) are obtained from the DFT calculations with the proper consideration of conformational distributions, all 27 second-order nonlinear susceptibility terms ($\chi^{(2)}_{ijk}$) can be calculated using eq 3. Then, $\chi^{(2)}_{\text{eff}}$ is obtained using eq 2 at a given polarization combination for a given tilt angle (θ) of the three-fold rotational axis of CH_3 with respect to the surface normal direction. Figure 2 plots the calculated $|\chi^{(2)}_{\text{eff}}|^2$ value, which is equivalent to the normalized SFG intensity, as a function of θ for the ssp, ppp, sps, and pss polarizations at the visible and IR beam incidence angles of 55 and 60°, respectively. These incidence angles were chosen because angles between 40 and 60° are commonly used in many SFG instruments.[50−53]

Figure 2a shows the data for the perfect C_{3v} point group, that is, methyl iodide, at a 2D surface. For the ssp signal, the symmetric stretch mode (A_1 mode) is peaked at θ = 0° and decays with the $\cos^2(\theta)$ function as θ increases; in contrast, the

https://doi.org/10.1021/acs.jpcb.3c03910
J. Phys. Chem. B 2023, 127, 8456−8467

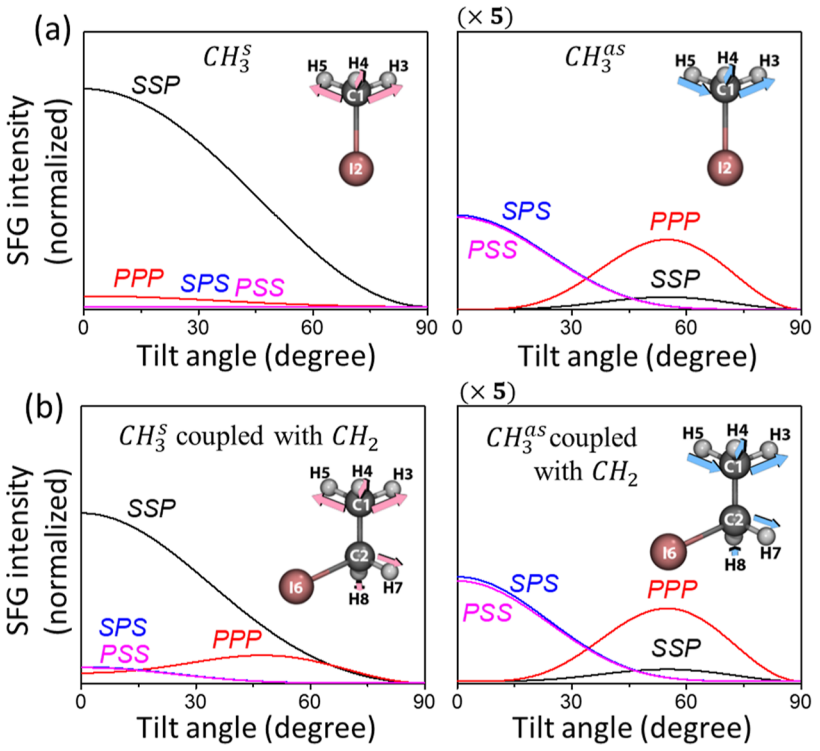

Figure 2. Comparison of the SFG intensities at ssp, ppp, sps, and pss polarizations for the (a) symmetric (A_1) and asymmetric (E) modes of the CH_3 group in CH_3I and the (b) normal modes containing symmetric and asymmetric stretches of the CH_3 group in CH_3CH_2I, as a function of the tilt angle (θ) of the CH_3 three-fold rotation axis with respect to the surface normal direction, calculated using the molecular hyperpolarizability tensors shown in Table 2. The calculation is for the case where the molecule is placed at the surface with the C_∞ symmetry. The incidence angles of I_{VIS} and I_{IR} were set to 55 and 60°, respectively, with respect to the surface normal direction. The asymmetric mode signals are multiplied with the factor shown at the top of the *y*-axis for comparison with the symmetric mode signals.

Table 3. Polarizability and Dipole Derivative Tensors of CH_3OH and CH_3CH_2OH[a]

	CH_3^s	CH_3^{as}
CH_3OH $\delta = 60°$	$\begin{pmatrix}-1.72 & 0.47 & 0.44\\ 0.47 & -2.33 & 0.24\\ 0.44 & 0.24 & -1.32\end{pmatrix}\begin{pmatrix}-2.35\\ -1.25\\ 7.83\end{pmatrix}$	$\begin{pmatrix}1.01 & -0.66 & -0.74\\ -0.66 & -1.02 & 1.37\\ -0.74 & 1.37 & -0.00\end{pmatrix}\begin{pmatrix}3.82\\ -7.01\\ 0.02\end{pmatrix}$
	CH_3^s coupled with CH_2	CH_3^{as} coupled with CH_2
CH_3CH_2OH $\delta = 60°$ and gauche	$\begin{pmatrix}-2.05 & -0.10 & -0.13\\ -0.10 & -2.43 & 0.17\\ -0.13 & 0.17 & -1.62\end{pmatrix}\begin{pmatrix}1.00\\ -1.29\\ 3.84\end{pmatrix}$	$\begin{pmatrix}-0.37 & 0.84 & 0.92\\ 0.84 & -0.40 & -0.15\\ 0.92 & -0.15 & -0.29\end{pmatrix}\begin{pmatrix}-4.56\\ 4.25\\ -0.15\end{pmatrix}$

[a]The three-fold rotation axis of the methyl group is aligned with the (vertical) *Z*-axis of the lab coordinate. For CH_3OH, only one of the staggered conformers is shown here with the C1−H4 atoms in the *YZ* plane. Other conformer values are shown in Table S3 in the Supporting Information. The tensor values shown here for CH_3CH_2OH are for the dihedral angle $\delta = 60°$ and the OH group in the gauche position with respect to the terminal CH_3 group. Other conformations of CH_3CH_2OH are shown in Table S3. The (3 × 3) matrix is $\left(\frac{\partial \alpha_{i'j'}}{\partial Q_q}\right)$, and the (3 × 1) matrix is $\left(\frac{\partial \mu_{k'}}{\partial Q_q}\right)$.

ssp signal of the asymmetric stretch mode (E mode) is zero at $\theta = 0°$ and peaked at $\theta = 54.74°$ and its magnitude is very small. This can be easily understood if one calculates the $\chi^{(2)}_{YYZ}$ tensor, which is the only $\chi^{(2)}_{ijk}$ component contributing to the ssp signal measured in a system with the C_∞ symmetry

$$\chi^{(2)}_{YYZ} = \frac{1}{4}\cos(\theta)[\beta_{aac} + \beta_{bbc} + (\beta_{aac} + \beta_{bbc})\cos^2(\theta) - (\beta_{aca} + \beta_{bcb} + \beta_{caa} + \beta_{cbb} - 2\beta_{ccc})\sin^2(\theta)] \quad (6)$$

This is essentially the numerator term in eq 3 for $\chi^{(2)}_{YYZ}$, which is obtained by simply applying the Euler transformation matrix to $\beta_{i',j',k'}$ and then integrating over all possible ψ and ϕ angles (from 0 to 2π). Using the $\beta_{i',j',k'}$ values of CH_3I in Table 2, the $\chi^{(2)}_{YYZ}$ component of the symmetric (A_1) and asymmetric (E) stretch mode is transformed in the following form

For the A_1 mode

$$\chi^{(2)}_{YYZ} = \frac{1}{4}\cos(\theta)[1.92 + 1.92\cos^2(\theta) + 2\sin^2(\theta)] \approx \cos(\theta) \quad (7)$$

For the E mode

$$\chi^{(2)}_{YYZ} = \frac{1}{4}\cos(\theta)[-1.08\sin^2(\theta)] = -0.27\cos(\theta)\sin^2(\theta) \quad (8)$$

https://doi.org/10.1021/acs.jpcb.3c03910
J. Phys. Chem. B 2023, 127, 8456−8467

Table 4. Hyperpolarizability $\beta_{i',j',k'}$ Tensors of CH_3OH and CH_3CH_2OH[a]

	CH_3^s	CH_3^{as}
CH_3OH	$\begin{pmatrix}0.00\\0.06\\\mathbf{1.57}\end{pmatrix}\begin{pmatrix}0.06\\0.00\\0.00\end{pmatrix}\begin{pmatrix}0.05\\0.00\\0.00\end{pmatrix}$ $\begin{pmatrix}0.06\\0.00\\0.00\end{pmatrix}\begin{pmatrix}0.00\\-0.06\\\mathbf{1.57}\end{pmatrix}\begin{pmatrix}0.00\\0.05\\0.00\end{pmatrix}$ $\begin{pmatrix}0.05\\0.00\\0.00\end{pmatrix}\begin{pmatrix}0.00\\0.05\\0.00\end{pmatrix}\begin{pmatrix}0.00\\0.00\\\mathbf{1.00}\end{pmatrix}$	$\begin{pmatrix}0.03\\\mathbf{0.47}\\0.00\end{pmatrix}\begin{pmatrix}\mathbf{0.47}\\-0.03\\0.00\end{pmatrix}\begin{pmatrix}\mathbf{0.58}\\0.00\\0.00\end{pmatrix}$ $\begin{pmatrix}\mathbf{0.47}\\-0.03\\0.00\end{pmatrix}\begin{pmatrix}-0.03\\\mathbf{-0.47}\\0.00\end{pmatrix}\begin{pmatrix}0.00\\\mathbf{0.58}\\0.00\end{pmatrix}$ $\begin{pmatrix}\mathbf{0.58}\\0.00\\0.00\end{pmatrix}\begin{pmatrix}0.00\\\mathbf{0.58}\\0.00\end{pmatrix}\begin{pmatrix}0.00\\0.00\\0.00\end{pmatrix}$
	CH_3^s coupled with CH_2	CH_3^{as} coupled with CH_2
CH_3CH_2OH	$\begin{pmatrix}0.00\\-1.19\\\mathbf{1.39}\end{pmatrix}\begin{pmatrix}-1.19\\0.00\\0.00\end{pmatrix}\begin{pmatrix}-0.87\\0.00\\0.00\end{pmatrix}$ $\begin{pmatrix}-1.19\\0.00\\0.00\end{pmatrix}\begin{pmatrix}0.00\\1.19\\\mathbf{1.39}\end{pmatrix}\begin{pmatrix}0.00\\-0.87\\0.00\end{pmatrix}$ $\begin{pmatrix}-0.87\\-0.01\\0.00\end{pmatrix}\begin{pmatrix}0.00\\-0.87\\0.00\end{pmatrix}\begin{pmatrix}0.00\\0.00\\\mathbf{1.00}\end{pmatrix}$	$\begin{pmatrix}0.29\\\mathbf{0.79}\\0.01\end{pmatrix}\begin{pmatrix}\mathbf{0.79}\\-0.29\\0.00\end{pmatrix}\begin{pmatrix}\mathbf{0.97}\\-0.26\\0.00\end{pmatrix}$ $\begin{pmatrix}\mathbf{0.79}\\-0.29\\0.00\end{pmatrix}\begin{pmatrix}-0.29\\\mathbf{-0.79}\\0.01\end{pmatrix}\begin{pmatrix}0.26\\\mathbf{0.97}\\0.00\end{pmatrix}$ $\begin{pmatrix}\mathbf{0.97}\\-0.26\\0.00\end{pmatrix}\begin{pmatrix}0.26\\\mathbf{0.97}\\0.00\end{pmatrix}\begin{pmatrix}0.00\\0.00\\0.01\end{pmatrix}$

[a]The tensor elements of CH_3OH are the weighted average of the *staggered* and *eclipsed* conformers. In the case of CH_3CH_2OH, the tensor elements are the weighted average of both *gauche* and trans orientations of the staggered conformers. The weighting factor is based on the Boltzmann statistics. The bold numbers are the terms expected to be large based on the perfect C_{3v} symmetry. All values are normalized with the β_{ccc} component of the symmetric stretch mode in which the CH_3 vibration is dominant. The tensor elements of individual conformers are shown in Table S4 in the Supporting Information.

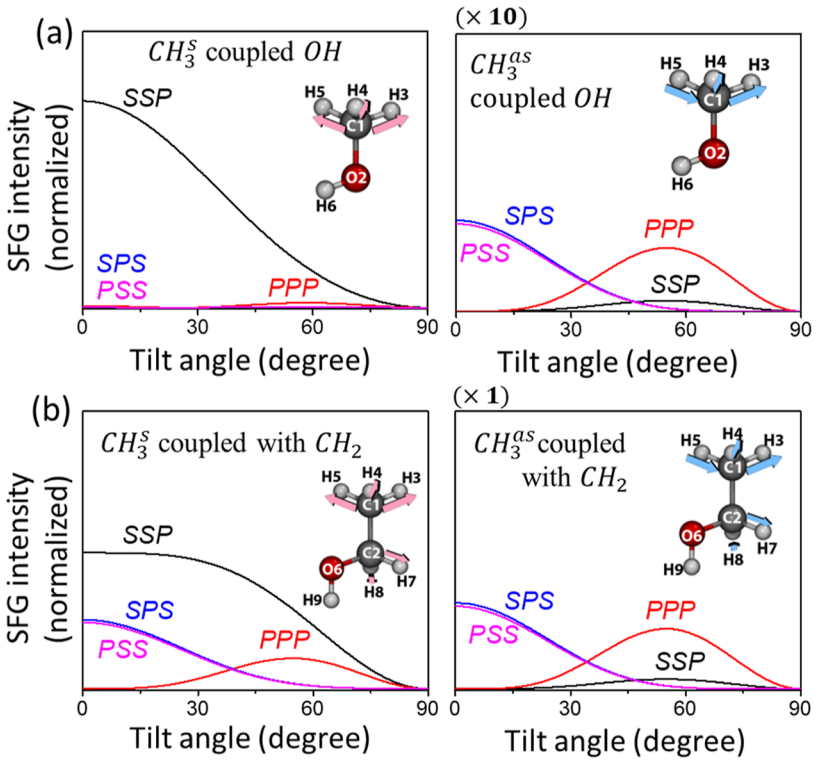

Figure 3. Comparison of the SFG intensities at ssp, ppp, sps, and pss polarizations for symmetric and asymmetric modes of the CH_3 group in (a) CH_3OH and (b) CH_3CH_2OH as a function of the tilt angle (θ) of the CH_3 three-fold rotation axis with respect to the surface normal direction, calculated using the molecular hyperpolarizability tensors shown in Table 4. The calculation is for the case where the molecule is placed at the surface with the C_∞ symmetry. The incidence angles of I_{VIS} and I_{IR} were set to 55 and 60°, respectively, with respect to the surface normal direction.

https://doi.org/10.1021/acs.jpcb.3c03910
J. Phys. Chem. B 2023, 127, 8456−8467

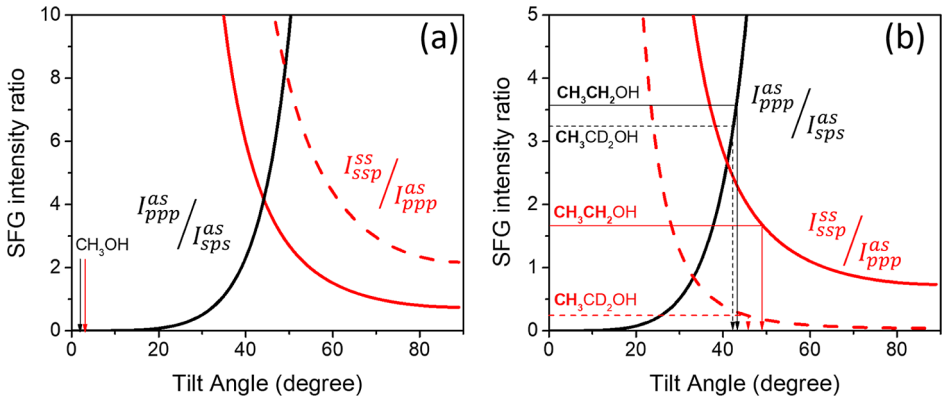

Figure 4. Relative intensities of the ssp signal of the ss mode versus the ppp signal of the as mode ($I^{ss}_{ssp}/I^{as}_{ppp}$) and the ppp versus sps signals of the as mode ($I^{as}_{ppp}/I^{as}_{sps}$) predicted for the air/liquid interface of (a) CH_3OH and (b) CH_3CH_2OH. The dashed lines are the prediction from the SBPD model using the R_s and R_a values from ref 54 (Table 5) and the solid lines are the prediction from the DFT calculations. The θ-dependence of the $I^{as}_{ppp}/I^{as}_{sps}$ ratio is essentially identical in both SBPD and DFT models. In (b), the solid and dotted horizonal lines indicate the $I^{ss}_{ssp}/I^{as}_{ppp}$ and $I^{as}_{ppp}/I^{as}_{sps}$ values experimentally determined for CH_3CH_2OH and CH_3CD_2OH, respectively.[54]

Note that the maximum of the $\cos(\theta)\sin^2(\theta)$ function is at θ = 54.74°, which equals the magic angle at which the orientation is indistinguishable from the random case. Similarly, the ppp signal of the asymmetric stretch mode is peaked at θ = 54.74°; in contrast, the sps and pss signals of the asymmetric stretch mode are peaked at θ = 0°.

In the case of ethyl iodide (Figure 2b), the coupling between the CH_3 and CH_2 stretch modes makes the tilt angle dependence of the SFG signal deviate from the perfect C_{3v} point group case. For that reason, the relative intensity difference between the symmetric and asymmetric stretch modes in the ssp spectrum becomes slightly smaller. The coupling with the CH_2 stretch makes the tilt angle dependence of the ppp signal of the CH_3 symmetric stretch mode quite different from that of the A_1 mode of the C_{3v} point group. For ethyl iodide, the ssp signal of the symmetric CH_3 stretch mode decays faster than the $\cos^2(\theta)$ function as θ increases.

SFG Calculations for Methanol and Ethanol. Using the same procedure shown in the iodide series, we have calculated the polarizability $\left(\frac{\partial \alpha_{i'j'}}{\partial Q_q}\right)$ and dipole $\left(\frac{\partial \mu_{k'}}{\partial Q_q}\right)$ derivatives of methanol and ethanol (Table 3), their molecular hyperpolarizability $\beta_{i',j',k'}$ tensors (Table 4), and the $|\chi^{(2)}_{eff}|^2$ term as a function of θ on a 2D surface for the ssp, ppp, sps, and pps polarizations at the visible and IR beam incidence angles of 55 and 60°, respectively (Figure 3).

In the case of CH_3OH (Table 3), the polarizability and dipole derivative tensor elements are larger than the values seen for CH_3I (Table 1). In the symmetric stretch mode, small non-zero values are noted in the derivative tensor elements that would be zero if it follows the A_1 mode of the C_{3v} point group. These differences and deviations are due to the coupling of the CH_3 stretch vibrations with the OH stretch, which breaks the C_{3v} symmetry (Figure 1). Consequently, the hyperpolarizability tensors of CH_3OH also have non-zero values in the elements that would be zero if the vibration is described by the A_1 mode of the C_{3v} point group (Table 4).

Similar to the CH_3CH_2I case, the polarizability and dipole derivative tensors as well as hyperpolarizability tensors of CH_3CH_2OH are all from the coupled vibrations of CH_3 and CH_2 in Tables 3 and 4, respectively. In the CH_3CH_2OH case, further coupling with OH makes non-zero values in the following terms of the hyperpolarizability (Table 4): $\beta_{aab} = \beta_{aba} = \beta_{baa} = -\beta_{bbb}$ and $\beta_{aca} = \beta_{bcb} = -\beta_{caa} = \beta_{cbb}$ in the symmetric mode and $\beta_{aaa} = -\beta_{abb} = -\beta_{bab} = -\beta_{bba}$ and $-\beta_{acb} = \beta_{bca} = -\beta_{cab} = \beta_{cba}$ in the asymmetric mode.

In the tilt angle (θ) dependence of CH_3OH (Figure 3a), the relative intensity difference of the ssp signal of the symmetric mode at θ = 0° and the ppp signal of the asymmetric mode at θ = 54.74° become smaller than the perfect C_{3v} case of CH_3I (Figure 2a). In the case of CH_3CH_2OH (Figure 3b), that difference is even smaller. The ssp signal of the CH_3OH symmetric stretch is still close to the $\cos^2(\theta)$ function, although its decay is slightly faster with θ (Figure 3a). In the case of CH_3CH_2OH (Figure 3b), the θ-dependence of the ssp signal of the mode involving the symmetric CH_3 stretch deviates quite significantly from the $\cos^2(\theta)$ function due to the intramolecular vibrational coupling with the CH_2OH group. Even the relative intensities of the sps and pss signals of the mode with the symmetric CH_3 stretch vibration become significant in the CH_3CH_2OH case.

Determining the Tilt Angle of the Terminal CH_3 Group at the Air/Liquid Interface. In order to determine the molecular tilt angle (θ) with respect to the surface normal direction, the experimentally measured SFG intensities are ratioed and compared with the theoretically predicted ratios. By taking the ratio, all parameters specific to experimental conditions are factored out, thus circumventing the difficulty of determining absolute intensity. In the literature, the ratio of the ssp signal of the symmetric stretch (ss) mode to the ppp signal of the asymmetric stretch (as) mode ($I^{ss}_{ssp}/I^{as}_{ppp}$) and the ratio of ppp to sps signals of the as mode ($I^{as}_{ppp}/I^{as}_{sps}$) were used.[19] The CH_3 ss and as modes appear at around 2860−2880 and 2960−2980 cm^{-1}, respectively.[50] Figure 4 plots these ratios, calculated from the alcohol data shown in Figure 3, as a function of the tilt angle of the CH_3 three-fold rotational axis. For comparison, the curves predicted from the SBPD model are also shown. The hyperpolarizability ratios used for the SBPD model prediction are shown in Table 5;[17,19,54] the corresponding values obtained from the DFT calculation are also listed for comparison in Table 5.

In Figure 4, the θ-dependence of the $I^{as}_{ppp}/I^{as}_{sps}$ ratio is practically indistinguishable in both SBPD and DFT models. However, the $I^{ss}_{ssp}/I^{as}_{ppp}$ ratio shows noticeably different θ-dependence between the two models. Based on the SBPD model and the I^{ss}_{ppp} values collected at different laser incidence

https://doi.org/10.1021/acs.jpcb.3c03910
J. Phys. Chem. B 2023, 127, 8456−8467

Table 5. Comparison of the Hyperpolarizability Ratio Used to Calculate the Relative SFG Intensities of the CH_3 ss and as Modes from Reference 54 and Those Obtained from DFT Calculations[a]

	SBPD[54]		DFT	
molecule	$R_s = \beta^{ss}_{aac}/\beta^{ss}_{ccc}$	$R_a = \beta^{as}_{aca}/\beta^{ss}_{ccc}$	$R_s = \beta^{ss}_{aac}/\beta^{ss}_{ccc}$	$R_a = \beta^{as}_{aca}/\beta^{ss}_{ccc}$
CH_3OH	1.7	0.37	1.57	0.58
CH_3CH_2OH			1.39	0.97
CH_3CD_2OH	3.4	4.55		
CH_3I			0.96	0.27
CH_3CH_2I			0.98	0.30

[a] R_s is needed to calculate the SFG intensity of the symmetric stretch mode, and R_a is needed to compare the relative intensities of the ss and as modes. See the example shown in eqs 6−8 for the ssp signal case.

angles, Gan et al. predicted that the tilt angle of the CH_3 group of methanol is close to zero at the air/liquid interface.[55] If the $I^{ss}_{ssp}/I^{as}_{ppp}$ ratio taken from the SFG spectra shown in their paper (Figure 3 in ref 55) is compared with the DFT calculation result (Figure 4a), the same conclusion is obtained. Based on molecular dynamics simulations, Zheng and Wei predicted the tilt angle of the CH_3 group of methanol to be ~23°.[30] At this angle, DFT calculation results predict $I^{as}_{ppp}/I^{as}_{sps}$ to be extremely small and $I^{ss}_{ssp}/I^{as}_{ppp}$ to be extremely large, which would be indistinguishable from the experimental values if experimental errors are considered.

In the case of ethanol, the I^{as}_{ppp} intensity is rather significant and thus the $I^{ss}_{ssp}/I^{as}_{ppp}$ ratio can be determined relatively meaningfully. For the CH_3CD_2OH system in which the CH_3 stretch modes can be decoupled from the CD_2 vibrations, Gan et al. measured $I^{as}_{ppp}/I^{as}_{sps} = 3.23$ and $I^{ss}_{ssp}/I^{as}_{ppp} = 0.25$.[19] Based on the SBPD model with the R_s and R_a values calculated from the experimentally measured Raman depolarization ratio (r) values of the corresponding vibration modes of CH_3CD_2OH (Table 5), Gan et al. determined the CH_3 tilt angle to be 42−45° from the surface normal direction.[19] They also reported that for CH_3CH_2OH, $I^{as}_{ppp}/I^{as}_{sps}$ and $I^{ss}_{ssp}/I^{as}_{ppp}$ are 3.53 and 1.67, respectively.[19] If those values are compared with the SBPD model in Figure 4b, it gives quite different tilt angles: 43° from $I^{as}_{ppp}/I^{as}_{sps}$ and 28° from $I^{ss}_{ssp}/I^{as}_{ppp}$. This discrepancy is due to the ignorance of the intramolecular coupling of the CH_3 and CH_2 groups. When the experimental values of CH_3CH_2OH are compared with the DFT model, then the predicted angle is 43−48°, which is in good agreement with the tilt angle determined with the SBPD model for CH_3CD_2OH.[54] These comparisons corroborate that the CH_3 stretch modes of ethanol cannot be described accurately if they are assumed to follow the C_{3v} symmetry; the coupling with the CH_2 group should not be ignored.

In the review paper by Wang et al., it was stated that the hyperpolarizability ratio (R_s) used in the SBPD model is different for the CH_3 group in different molecules: 1.7 for CH_3OH, 3.4 for CH_3CH_nOH ($n \geq 1$), 1.9 for $(CH_3)_2C{=}O$, and 2.3 for $(CH_3)_2S{=}O$.[17] But the detailed reason was not discussed. Also, empirical R_a values are not known for most molecules, which makes it difficult to compare the relative intensities between the symmetric and asymmetric modes. We propose that the DFT calculation results of the CH_3I case can be used for the SFG analysis of the CH_3- group in a system where vibrational coupling is negligible, and the CH_3CH_2I results can be used for analysis of the CH_3CH_2- group without coupling to a polar functional group. For the comparison purpose, the $I^{as}_{ppp}/I^{as}_{sps}$ and $I^{ss}_{ssp}/I^{as}_{ppp}$ ratios calculated from the data shown in Figures 2 and 3 are plotted in Figure 5. Note that these are the calculation results obtained with the delta function assumption for the tilt angle distribution.

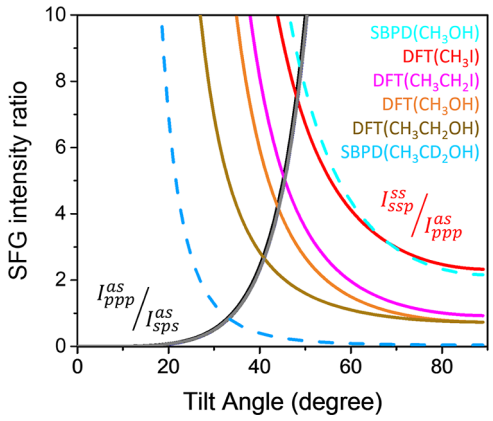

Figure 5. Relative intensities of the ssp signal of the ss mode versus the ppp signal of the as mode ($I^{ss}_{ssp}/I^{as}_{ppp}$) and the ppp versus sps signals of the as mode ($I^{as}_{ppp}/I^{as}_{sps}$) predicted for the CH_3-group of CH_3I, CH_3CH_2I, CH_3OH, and CH_3CH_2OH placed in the 2D interface with the C_∞ symmetry. The solid lines are the prediction from DFT calculations, and the dashed lines are the prediction from the SBPD model using the R_s and R_a values from ref 54. The $I^{as}_{ppp}/I^{as}_{sps}$ ratios of the two models are practically identical. Note that, in this calculation, the tilt angle distribution is assumed to be the delta function.

Figure 5 provides several insights that are important for experimental design and data interpretation. Since the I^{as}_{ppp} intensity decays to zero as θ decreases to 0° and the I^{ss}_{ssp} intensity decays to zero as θ approaches 90° (as shown in Figures 2 and 3), it would be difficult to measure their signals accurately (at least subject to error in experimental measurements or peak fitting) if the tilt angle of the molecule is in these extremes. Thus, the tilt angle below 20° and above 70° would be difficult to determine accurately. Note that this does not mean that the values determined to be in these ranges are meaningless; it just means that the precision is significantly limited, and any physical interpretation should be done while keeping this limitation in mind.

When the $I^{ss}_{ssp}/I^{as}_{ppp}$ ratio is used, the tilt angle deduced from the experimental data is highly dependent on the model chosen for analysis. If the CH_3 stretch modes are not coupled with the vibrations of the rest of molecule, then the analysis can be done with the curve obtained with the DFT calculation of methyl iodide. This curve can be generated with the SBPD model using the R_s and R_a values for methyl iodide (i.e., 0.96 and 0.27, respectively) in Table 5. Note that this curve nearly overlaps with the SBPD model using the R_s and R_a values for methanol taken from ref 54 (i.e., 1.7 and 0.37, respectively, as shown in Table 5). The difference in tilt angle determined with these two methods would be practically negligible (Figure 5). If the CH_3 stretch vibrations are coupled with the CH_2 stretch vibrations, then the curve obtained with the DFT calculation of ethyl iodide (which can be reproduced with the SBPD model using the R_s = 0.98 and R_a = 0.30 values for ethyl iodide in Table 5) could be used. If additional coupling of CH_3 occurs with the next nearest group (in ethanol, it is the OH group), then the $I^{ss}_{ssp}/I^{as}_{ppp}$ ratio curve can shift down further from the theoretical curve calculated with the ideal C_{3v} symmetry assumption. Of course,

https://doi.org/10.1021/acs.jpcb.3c03910
J. Phys. Chem. B 2023, 127, 8456−8467

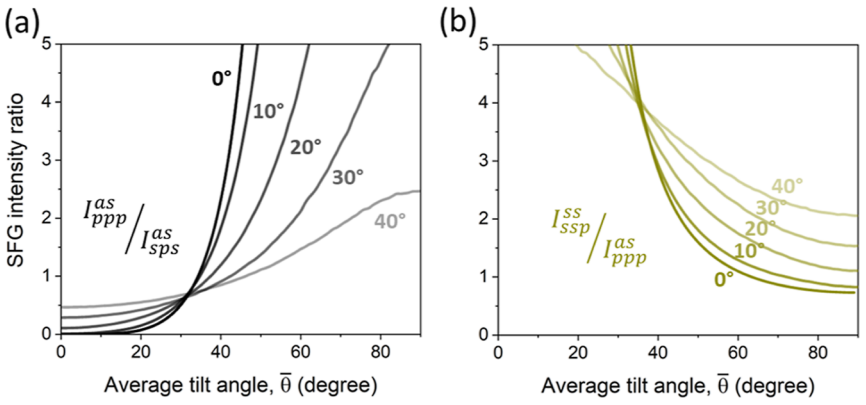

Figure 6. SFG intensity ratio for (a) ppp versus sps signals of the as mode ($I^{as}_{ppp}/I^{as}_{sps}$) and (b) ssp signal of the ss mode versus the ppp signal of the as mode ($I^{ss}_{ssp}/I^{as}_{ppp}$) predicted for the air/liquid interface of CH_3CH_2OH having the Gaussian distribution of tilt angle with the standard deviation of $\sigma = 0$, 10, 20, 30, and 40°.

the hydrogen bonding interactions of the hydroxyl group of ethanol at the air/liquid interface with other molecules underneath would affect the dynamics in vibrational coupling with the stretch mode of the terminal CH_3 group, which was not studied in this work and will be the subject of a future study.

Another important parameter to take into account is the tilt angle distribution. So far, we have discussed the tilt angle dependence of SFG intensities without considering the tilt angle distribution (i.e., using the delta function) to make the degree of freedom minimum for the simplicity. But in reality, molecules exposed at the interface will have a broad distribution of tilt angles, which is governed by thermal equilibrium at a given temperature.[56,57] So, the additional degree of freedom should be included in the theoretical calculation of the SFG intensity, which is the statistical distribution of tilt angles. This calculation can be done by multiplying the Gaussian distribution function when the Euler matrix term is integrated in eq 3. Figure 6 plots the dependences of $I^{as}_{ppp}/I^{as}_{sps}$ and $I^{ss}_{ssp}/I^{as}_{ppp}$ on the average tilt angle, $\bar{\theta}$, for the air/ethanol interface, assuming that the tilt angle has the Gaussian distribution with standard deviation (σ) of 0, 10, 20, 30, and 40°. The results show that as the tilt angle distribution becomes broader (i.e., larger σ), the θ-dependence of $I^{ss}_{ssp}/I^{as}_{ppp}$ and $I^{as}_{ppp}/I^{as}_{sps}$ becomes weaker.[19,58]

Note that all calculations done in this study were carried out without considering the peak broadening of the observed vibrational mode, i.e., the damping factor (Γ_q) in the denominator of eq 3. In the case of methanol, the hydrogen bonding interactions of the neighboring OH groups in the liquid phase may affect the damping of the stretch vibration of the CH_3 group exposed to the air side because these stretch vibrations are coupled (see Movies 1, 2, 3, and 4 in the Supporting Information). In addition, the Fermi resonance with overtones of the bending modes will also affect the polarizability and dipole tensors of the stretch modes,[31,32] which were not modeled in our DFT calculations. Considering all these factors, which include vibrational coupling with neighboring groups, Fermi resonance, peak broadening, tilt angle distribution, and experimental noises, it would be difficult to compare the absolute values determined from different molecular systems. If simple molecules like the ones considered in this study are not as simple as one may think, analysis of polymer surfaces or multicomponent systems would be even more complicated. Thus, one may have to limit the comparison of experimental data only to the relative trends or magnitudes determined among a homologous series within the validity of specific assumptions made for the data interpretation.

CONCLUSIONS

The DFT-based calculations of SFG peak intensity for the CH_3 stretch modes of CH_3I, CH_3CH_2I, CH_3OH, and CH_3CH_2OH were used to investigate the effect of vibrational coupling of the CH_3 stretch modes with neighboring CH_2 and OH groups for the molecules at the 2D interface with the C_∞ symmetry. The DFT calculations showed that the polarizability and dipole derivative tensors of the CH_3 stretch modes have non-zero values in the terms that should be zero in the C_{3v} point group, except the CH_3I case. These terms are not completely cancelled out by the random distribution in the azimuth and twist angles. For that reason, the tilt angle dependence of the $I^{ss}_{ssp}/I^{as}_{ppp}$ ratio calculated for the CH_3OH and CH_3CH_2OH molecules is quite different from that calculated from the SBPD model for these molecules. In contrast, the tilt angle dependence of the SFG intensity ratio of the same mode at different polarizations, for example, $I^{as}_{ppp}/I^{as}_{sps}$, is not affected much by the vibrational coupling. The DFT calculation results provided new values for the hyperpolarizability ratios ($R_s = \beta^{ss}_{aac}/\beta^{ss}_{ccc}$ and $R_a = \beta^{as}_{aca}/\beta^{ss}_{ccc}$) that could be used to predict the tilt angle dependence of the SFG peak intensities of CH_3 groups in other hydrocarbons; but these values should be used keeping in mind that many other molecular and experimental parameters limit the accuracy of the prediction.

ASSOCIATED CONTENT

Supporting Information

The Supporting Information is available free of charge at https://pubs.acs.org/doi/10.1021/acs.jpcb.3c03910.

DFT-calculated energies for CH_3OH and CH_3CH_2OH (convergence criteria and basis set effects); DFT-calculated IR and Raman spectra for CH_3I and CH_3CH_2I (basis set effects); description of normal modes observed in DFT-predicted spectra of CH_3I, CH_3OH, CH_3CH_2I, and CH_3CH_2OH; DFT-calculated IR and Raman spectra for CH_3I, CH_3CH_2I, CH_3OH, and CH_3CH_2OH; DFT-calculated IR and Raman spectra for CH_3OH and CH_3CH_2OH with different incident wavelengths; DFT-calculated energies for CH_3OH and CH_3CH_2OH (conformer effects); example of calculating the derivative tensors of two rotational conformers of CH_3OH; and polarizability derivative, dipole derivative, and hyperpolarizability tensors of CH_3I, CH_3CH_2I, CH_3OH, and CH_3CH_2OH (PDF)

https://doi.org/10.1021/acs.jpcb.3c03910
J. Phys. Chem. B 2023, 127, 8456−8467

Stretching vibrations of normal modes for methyl iodide (MP4)

Stretching vibrations of normal modes for ethyl iodide (MP4)

Stretching vibrations of normal modes for methanol (MP4)

Stretching vibrations of normal modes for ethanol (MP4)

Mathematica Code for the SFG intensity calculation of methanol (PDF)

AUTHOR INFORMATION

Corresponding Author

Seong H. Kim − *Department of Chemical Engineering and Materials Research Institute, Pennsylvania State University, University Park, Pennsylvania 16802, United States;* orcid.org/0000-0002-8575-7269; Email: shk10@psu.edu

Authors

Juseok Choi − *Department of Chemical Engineering and Materials Research Institute, Pennsylvania State University, University Park, Pennsylvania 16802, United States;* orcid.org/0000-0002-0988-6544

Albert L. Kwansa − *Department of Materials Science and Engineering, North Carolina State University, Raleigh, North Carolina 27695, United States*

Yaroslava G. Yingling − *Department of Materials Science and Engineering, North Carolina State University, Raleigh, North Carolina 27695, United States;* orcid.org/0000-0002-8557-9992

Complete contact information is available at: https://pubs.acs.org/10.1021/acs.jpcb.3c03910

Notes

The authors declare no competing financial interest.

ACKNOWLEDGMENTS

This work was supported as part of the Center for Lignocellulose Structure and Formation, an Energy Frontier Research Center funded by the U.S. Department of Energy, Office of Science, Basic Energy Sciences (award no: DESC0001090) and in part by the National Science Foundation (grant no: CHEM-2203635).

REFERENCES

(1) Shen, Y.-R. *The Principles of Nonlinear Optics*; John Wiley & Sons, 1984.

(2) Lambert, A. G.; Davies, P. B.; Neivandt, D. J. Implementing the Theory of Sum Frequency Generation Vibrational Spectroscopy: A Tutorial Review. *Appl. Spectrosc. Rev.* **2005**, *40*, 103−145.

(3) Shen, Y. R. Basic Theory of Surface Sum-Frequency Generation. *J. Phys. Chem. C* **2012**, *116*, 15505−15509.

(4) Shen, Y. R. Revisiting the basic theory of sum-frequency generation. *J. Chem. Phys.* **2020**, *153*, 180901.

(5) Li, X.; Rupprechter, G. Sum frequency generation spectroscopy in heterogeneous model catalysis: a minireview of CO-related processes. *Catal. Sci. Technol.* **2021**, *11*, 12−26.

(6) Lu, X.; Clarke, M. L.; Li, D.; Wang, X.; Xue, G.; Chen, Z. A Sum Frequency Generation Vibrational Study of the Interference Effect in Poly(n-butyl methacrylate) Thin Films Sandwiched between Silica and Water. *J. Phys. Chem. C* **2011**, *115*, 13759−13767.

(7) Franz, J.; van Zadel, M.-J.; Weidner, T. A trough for improved SFG spectroscopy of lipid monolayers. *Rev. Sci. Instrum.* **2017**, *88*, 053106.

(8) de Aguiar, H. B.; Strader, M. L.; de Beer, A. G. F.; Roke, S. Surface Structure of Sodium Dodecyl Sulfate Surfactant and Oil at the Oil-in-Water Droplet Liquid/Liquid Interface: A Manifestation of a Nonequilibrium Surface State. *J. Phys. Chem. B* **2011**, *115*, 2970−2978.

(9) Rocha-Mendoza, I.; Yankelevich, D. R.; Wang, M.; Reiser, K. M.; Frank, C. W.; Knoesen, A. Sum Frequency Vibrational Spectroscopy: The Molecular Origins of the Optical Second-Order Nonlinearity of Collagen. *Biophys. J.* **2007**, *93*, 4433−4444.

(10) Barnette, A. L.; Bradley, L. C.; Veres, B. D.; Schreiner, E. P.; Park, Y. B.; Park, J.; Park, S.; Kim, S. H. Selective Detection of Crystalline Cellulose in Plant Cell Walls with Sum-Frequency-Generation (SFG) Vibration Spectroscopy. *Biomacromolecules* **2011**, *12*, 2434−2439.

(11) Ogawa, Y.; Lee, C. M.; Nishiyama, Y.; Kim, S. H. Absence of Sum Frequency Generation in Support of Orthorhombic Symmetry of α-Chitin. *Macromolecules* **2016**, *49*, 7025−7031.

(12) Mizutani, G.; Koyama, T.; Tomizawa, S.; Sano, H. Distinction between some saccharides in scattered optical sum frequency intensity images. *Spectrochim. Acta, Part A* **2005**, *62*, 845−849.

(13) Tyrode, E.; Hedberg, J. A Comparative Study of the CD and CH Stretching Spectral Regions of Typical Surfactants Systems Using VSFS: Orientation Analysis of the Terminal CH3 and CD3 Groups. *J. Phys. Chem. C* **2012**, *116*, 1080−1091.

(14) Gan, W.; Wu, D.; Zhang, Z.; Feng, R.-r.; Wang, H.-f. Polarization and experimental configuration analyses of sum frequency generation vibrational spectra, structure, and orientational motion of the air/water interface. *J. Chem. Phys.* **2006**, *124*, 114705.

(15) Richmond, G. L. Molecular Bonding and Interactions at Aqueous Surfaces as Probed by Vibrational Sum Frequency Spectroscopy. *Chem. Rev.* **2002**, *102*, 2693−2724.

(16) Saito, K.; Peng, Q.; Qiao, L.; Wang, L.; Joutsuka, T.; Ishiyama, T.; Ye, S.; Morita, A. Theoretical and experimental examination of SFG polarization analysis at acetonitrile−water solution surfaces. *Phys. Chem. Chem. Phys.* **2017**, *19*, 8941−8961.

(17) Wang, H. F.; Gan, W.; Lu, R.; Rao, Y.; Wu, B. H. Quantitative spectral and orientational analysis in surface sum frequency generation vibrational spectroscopy (SFG-VS). *Int. Rev. Phys. Chem.* **2005**, *24*, 191−256.

(18) Choi, J.; Lee, J.; Makarem, M.; Huang, S.; Kim, S. H. Numerical Simulation of Vibrational Sum Frequency Generation Intensity for Non-Centrosymmetric Domains Interspersed in an Amorphous Matrix: A Case Study for Cellulose in Plant Cell Wall. *J. Phys. Chem. B* **2022**, *126*, 6629−6641.

(19) Gan, W.; Zhang, Z.; Feng, R.-r.; Wang, H.-f. Spectral Interference and Molecular Conformation at Liquid Interface with Sum Frequency Generation Vibrational Spectroscopy (SFG-VS). *J. Phys. Chem. C* **2007**, *111*, 8726−8738.

(20) Hirose, C.; Akamatsu, N.; Domen, K. Formulas for the analysis of surface sum-frequency generation spectrum by CH stretching modes of methyl and methylene groups. *J. Chem. Phys.* **1992**, *96*, 997−1004.

(21) Hirose, C.; Yamamoto, H.; Akamatsu, N.; Domen, K. Orientation analysis by simulation of vibrational sum frequency generation spectrum: CH stretching bands of the methyl group. *J. Phys. Chem.* **1993**, *97*, 10064−10069.

(22) Zhang, D.; Gutow, J.; Eisenthal, K. Vibrational spectra, orientations, and phase transitions in long-chain amphiphiles at the air/water interface: Probing the head and tail groups by sum frequency generation. *J. Phys. Chem.* **1994**, *98*, 13729−13734.

(23) Yamamoto, H.; Akamatsu, N.; Wada, A.; Domen, K.; Hirose, C. The orientation analysis from polarization characteristics of the surface vibrational SFG spectrum of HCO2 on MgO(001) surface. *J. Electron Spectrosc. Relat. Phenom.* **1993**, *64*−*65*, 507−513.

(24) Tong, Y.; Zhang, I. Y.; Campen, R. K. Experimentally quantifying anion polarizability at the air/water interface. *Nat. Commun.* **2018**, *9*, 1313.

(25) Vincent, A. *Molecular Symmetry and Group Ttheory: A Programmed Introduction to Chemical Applications*; John Wiley & Sons, 2013.

(26) Atkins, P.; Atkins, P. W.; de Paula, J. *Physical Chemistry*; Oxford University Press, 2014.

(27) Yu, Y.; Lin, K.; Zhou, X.; Wang, H.; Liu, S.; Ma, X. New C−H Stretching Vibrational Spectral Features in the Raman Spectra of Gaseous and Liquid Ethanol. *J. Phys. Chem. C* **2007**, *111*, 8971−8978.
(28) Wang, L.; Ishiyama, T.; Morita, A. Theoretical Investigation of C−H Vibrational Spectroscopy. 1. Modeling of Methyl and Methylene Groups of Ethanol with Different Conformers. *J. Phys. Chem. A* **2017**, *121*, 6687−6700.
(29) Wang, L.; Ishiyama, T.; Morita, A. Theoretical Investigation of C−H Vibrational Spectroscopy. 2. Unified Assignment Method of IR, Raman, and Sum Frequency Generation Spectra of Ethanol. *J. Phys. Chem. A* **2017**, *121*, 6701−6712.
(30) Zheng, R.-H.; Wei, W.-M. Sum-frequency vibrational spectroscopy of methanol at interfaces due to Fermi resonance. *Phys. Chem. Chem. Phys.* **2022**, *24*, 27204−27211.
(31) Chen, X.; Lee, C. M.; Wang, H.-F.; Jensen, L.; Kim, S. H. Experimental and Theoretical Study of Azimuth Angle and Polarization Dependences of Sum-Frequency-Generation Vibrational Spectral Features of Uniaxially Aligned Cellulose Crystals. *J. Phys. Chem. C* **2017**, *121*, 18876−18886.
(32) Lee, C. M.; Chen, X.; Weiss, P. A.; Jensen, L.; Kim, S. H. Quantum Mechanical Calculations of Vibrational Sum-Frequency-Generation (SFG) Spectra of Cellulose: Dependence of the CH and OH Peak Intensity on the Polarity of Cellulose Chains within the SFG Coherence Domain. *J. Phys. Chem. Lett.* **2017**, *8*, 55−60.
(33) Gualtieri, E. J.; Haupert, L. M.; Simpson, G. J. Interpreting nonlinear optics of biopolymer assemblies: Finding a hook. *Chem. Phys. Lett.* **2008**, *465*, 167−174.
(34) Xiao, D.; Fu, L.; Liu, J.; Batista, V. S.; Yan, E. C. Y. Amphiphilic Adsorption of Human Islet Amyloid Polypeptide Aggregates to Lipid/Aqueous Interfaces. *J. Mol. Biol.* **2012**, *421*, 537−547.
(35) Carr, J. K.; Wang, L.; Roy, S.; Skinner, J. L. Theoretical Sum Frequency Generation Spectroscopy of Peptides. *J. Phys. Chem. B* **2015**, *119*, 8969−8983.
(36) Superfine, R.; Huang, J. Y.; Shen, Y. R. Experimental determination of the sign of molecular dipole moment derivatives: an infrared—visible sum frequency generation absolute phase measurement study. *Chem. Phys. Lett.* **1990**, *172*, 303−306.
(37) Frisch, M. J.; Pople, J. A.; Binkley, J. S. Self-consistent molecular orbital methods 25. Supplementary functions for Gaussian basis sets. *J. Chem. Phys.* **1984**, *80*, 3265−3269.
(38) Becke, A. D. Density-functional thermochemistry. III. The role of exact exchange. *J. Chem. Phys.* **1993**, *98*, 5648−5652.
(39) Krishnan, R.; Binkley, J. S.; Seeger, R.; Pople, J. A. Self-consistent molecular orbital methods. XX. A basis set for correlated wave functions. *J. Chem. Phys.* **1980**, *72*, 650−654.
(40) Wadt, W. R.; Hay, P. J. Ab initio effective core potentials for molecular calculations. Potentials for main group elements Na to Bi. *J. Chem. Phys.* **1985**, *82*, 284−298.
(41) Igel-Mann, G.; Stoll, H.; Preuss, H. Pseudopotentials for main group elements (IIIa through VIIa). *Mol. Phys.* **1988**, *65*, 1321−1328.
(42) Gaussian. Description of the Freq keyword (G16 Rev. C.01). https://gaussian.com/freq/ (accessed July 24, 2023).
(43) Dennington, R.; Keith, T. A.; Millam, J. M. *GaussView (Version 6)*; Semichem Inc.: Shawnee Mission KS, 2016.
(44) O'boyle, N. M.; Tenderholt, A. L.; Langner, K. M. cclib: A library for package-independent computational chemistry algorithms. *J. Comput. Chem.* **2008**, *29*, 839−845.
(45) Colles, M. J.; Griffiths, J. E. Relative and Absolute Raman Scattering Cross Sections in Liquids. *J. Chem. Phys.* **1972**, *56*, 3384−3391.
(46) https://github.com/gausssum/gausssum (accessed July 24, 2023).
(47) Raab, M.; Becca, J. C.; Heo, J.; Lim, C.-K.; Baev, A.; Jensen, L.; Prasad, P. N.; Velarde, L. Doubly resonant sum frequency spectroscopy of mixed photochromic isomers on surfaces reveals conformation-specific vibronic effects. *J. Chem. Phys.* **2019**, *150*, 114704.
(48) Kahn, K.; Bruice, T. C. Focal-Point Conformational Analysis of Ethanol, Propanol, and Isopropanol. *ChemPhysChem* **2005**, *6*, 487−495.
(49) Carballeira, L.; Pereiras, A. J.; Rios, M. A. Design and application of a molecular mechanics force field for alkyl iodides including an electrostatic polarization model. *J. Comput. Chem.* **1990**, *11*, 734−742.
(50) Lu, R.; Gan, W.; Wu, B.-h.; Zhang, Z.; Guo, Y.; Wang, H.-f. C−H Stretching Vibrations of Methyl, Methylene and Methine Groups at the Vapor/Alcohol (n = 1−8) Interfaces. *J. Phys. Chem. B* **2005**, *109*, 14118−14129.
(51) Lu, R.; Gan, W.; Wu, B.-h.; Chen, H.; Wang, H.-f. Vibrational Polarization Spectroscopy of CH Stretching Modes of the Methylene Group at the Vapor/Liquid Interfaces with Sum Frequency Generation. *J. Phys. Chem. B* **2004**, *108*, 7297−7306.
(52) Weidner, T.; Apte, J. S.; Gamble, L. J.; Castner, D. G. Probing the Orientation and Conformation of α-Helix and β-Strand Model Peptides on Self-Assembled Monolayers Using Sum Frequency Generation and NEXAFS Spectroscopy. *Langmuir* **2010**, *26*, 3433−3440.
(53) Pickering, J. D.; Bregnhøj, M.; Chatterley, A. S.; Rasmussen, M. H.; Roeters, S. J.; Strunge, K.; Weidner, T. Tutorials in vibrational sum frequency generation spectroscopy. II. Designing a broadband vibrational sum frequency generation spectrometer. *Biointerphases* **2022**, *17*, 011202.
(54) Wu, H.; Zhang, W.-k.; Gan, W.; Cui, Z.-f.; Wang, H.-f. An empirical approach to the bond additivity model in quantitative interpretation of sum frequency generation vibrational spectra. *J. Chem. Phys.* **2006**, *125*, 133203.
(55) Gan, W.; Wu, B.-h.; Zhang, Z.; Guo, Y.; Wang, H.-f. Vibrational Spectra and Molecular Orientation with Experimental Configuration Analysis in Surface Sum Frequency Generation (SFG). *J. Phys. Chem. C* **2007**, *111*, 8716−8725.
(56) Tarek, M.; Tobias, D. J.; Klein, M. L. Molecular dynamics investigation of the surface/bulk equilibrium in an ethanol−water solution. *J. Chem. Soc., Faraday Trans.* **1996**, *92*, 559−563.
(57) Sokhan, B. V. P.; Tildesley, D. J. The free surface of water: molecular orientation, surface potential and nonlinear susceptibility. *Mol. Phys.* **1997**, *92*, 625−640.
(58) Simpson, G. J.; Rowlen, K. L. An SHG Magic Angle: Dependence of Second Harmonic Generation Orientation Measurements on the Width of the Orientation Distribution. *J. Am. Chem. Soc.* **1999**, *121*, 2635−2636.

https://doi.org/10.1021/acs.jpcb.3c03910
J. Phys. Chem. B 2023, 127, 8456−8467